

Numerical Simulation and Optimization of Forced Convection Heat Transfer of Magnetic Nanofluid in a Channel in the Presence of a Non-Uniform Magnetic Field

M. Goharkhah^{1*}, M. Esmaili² and M. Ashjaee³

1. Department of Mechanical Engineering, Sahand University of Technology
2, 3. Department of Mechanical Engineering, Faculty of Engineering, Kharazmi University

*Postal Code: 51335/1996, Tabriz, IRAN

Goharkhah@ut.ac.ir

In this paper, the effect of an external non-uniform magnetic field on forced convective heat transfer of magnetite nanofluid (ferrofluid) in a heated channel is studied numerically. The main goal is to emphasize the importance of magnetic field location and investigate the possibility of heat transfer enhancement by finding the optimum location of magnetic field source. It is observed that the magnetic field results in creation of recirculation zones which affect the thermal boundary layer thickness and Nusselt number. Results show that the effect of magnetic field location on the heat transfer is completely dependent on the thermal boundary condition. It is also shown that the flow and temperature fields can be manipulated by application of multiple magnetic field sources. Using genetic algorithm (GA), an optimum arrangement for locations of eight magnetic field sources is obtained resulting in a 27% heat transfer enhancement compared to the case of no magnetic field.

Keywords: Heat transfer; Forced convection, Ferrofluid, Mini channel, Magnetic field, Optimization, Genetic algorithm

Nomenclature

B magnetic flux density (T)
C_p specific heat (J/kgK)
 \vec{F}_k magnetic body force (N)
H magnetic field (A/m)
i, j unit vectors (horizontal , vertical)
L channel length (m)
m strength of the magnetic field, (Am)
M magnetization (A/m)
Nu Nusselt number
P Pressure (Pa)
Pr Prantdl number ($Pr = \nu/\alpha$)
r radial direction (m)

T Temperature (K)
t Time (s)
V_m scalar magnetic potential
u, v fluid velocities (horizontal , vertical, m/s)
W channel height (m)
X, Y locations of a single line dipole, m
x, y Cartesian coordinates (horizontal , vertical, m)
 α thermal diffusivity (m^2 / s)
 β volumetric expansion coefficient ($1/ K$)
 θ viscous dissipation
 μ dynamic viscosity ($kg/m s$)
 μ_0 magnetic permeability invacuum ($4\pi \times 10^{-7} \frac{N}{A^2}$)
 ρ density (kg/m^3)
 ϕ polar angle (rad)
 χ_m magnetic susceptibility

Subscripts

ref reference condition

1. Assistant Professor (Corresponding Author)
2. Assistant Professor
3. Professor

0	at reference temperature (300 K)
H	related to heated inlet
m	mean value

Introduction

Ferrofluid is a colloidal liquid made of nanoscale magnetic particles suspended in a carrier liquid typically water or oil [1]. It becomes strongly magnetized in the presence of an external magnetic field. Thus, it is possible to alter the ferrofluid flow field and temperature distribution, increase flow mixing, disturb the thermal boundary layer and consequently improve the heat transfer rate. Due to this distinguished characteristic, ferrofluid has been utilized in several applications such as micro-scale heat exchangers in MEMS devices, bioengineering, aerospace, and electronic cooling of spacecraft devices in microgravity condition [2-4].

One of the most serious problems in designing spacecraft equipments is reliable heat removal in low and micro-gravity conditions. Due to the lack of gravity, conventional coolants cannot be circulated around the heat dissipating devices appropriately. Thus, ferrofluid can be a good alternative. The magnetic force resulted from the external magnetic field can drive the ferrofluid to the heat source, circulate around it and facilitate the heat transfer process.

Numerical study of ferrofluid flow and heat transfer has been growing rapidly in the recent years. Ferrofluid thermomagnetic convection in which ferrofluid is confined in an enclosure and is subjected to a magnetic field has been considered in numerical and experimental studies with a variety of geometries and thermal boundary conditions [5-8].

A group of studies have also concentrated on forced convection heat transfer problem [9-13]. Ganguly et al. [11] numerically studied two-dimensional forced convection heat transfer of a hot ferrofluid flowing through a channel with a cold wall under the influence of a line-source dipole. It was shown that the local vortex resulted from the magnetic field alters the advection energy transport and enhances heat transfer. Streck and Jopek [12] studied the two-dimensional and time dependent heat transfer of a ferrofluid in a channel with isothermal walls under the influence of a magnetic dipole located below the channel. They showed that an imposed thermal gradient produces a spatial variation in the magnetization through the temperature - dependent magnetic susceptibility for ferrofluids and therefore renders the Kelvin body force non-uniform spatially. Xuan et al. [13] calculated flow and temperature distribution of a ferrofluid in a micro-channel with adiabatic and isothermal walls using lattice-Boltzmann method. In their work, the magnetic force was considered a constant and it was shown that heat transfer

augmentation depends on the magnitude and direction of the magnetic force. Aminfar et al. [9] studied the forced convection of ferrofluid in a duct under the influence of a transverse non-uniform magnetic field which is generated by an electric current going through a wire parallel to the duct. They reported a considerable enhancement of average heat transfer coefficient in their studied case.

Goharkhah and Ashjaee [14] and Ghasemian et al. [15] investigated the influence of alternating magnetic field on the convective heat transfer of ferrofluid and showed that the intensity and frequency of the external magnetic field has a significant effect on heat transfer. Sheikhnejad et al. [16] studied different magnetic field distributions on laminar ferroconvection heat transfer in horizontal tube. They showed that the magnetic field causes an increase in both pressure loss and heat transfer. The magnetic field with low gradient and high intensity was shown to be the best choice for both saving energy and heat transfer enhancement. Sheikhnejad et al. [17] also carried out a three-dimensional numerical analysis of ferrofluid flow through a horizontal tube under the influence of two fixed parallel magnet bars.

Additionally, several numerical studies have concentrated on biomagnetic fluid dynamics (BFD) considering blood as a magnetic fluid [18-20]. Despite several numerical studies, the mechanism of ferrofluid heat transfer is not still clearly investigated. Moreover, any study concerning the effect of magnetic field location on heat transfer and the optimization problem has not been reported previously.

In the current study, forced convection heat transfer of ferrofluid in a heated channel under an external non-uniform magnetic field is studied numerically. The effect of magnetic field location on the heat transfer rate has been investigated for two common boundary conditions of constant temperature and constant heat flux. Furthermore, the optimum locations of multiple magnetic field sources and heat transfer enhancement have been calculated using genetic algorithm.

Problem Description

Ferrofluid flows through a two-dimensional channel with an insulated top and a heated bottom surface. The channel height and length are $W=2\text{mm}$ and $L=20\text{mm}$, respectively. A non-uniform two-dimensional magnetic field is created by a magnetic dipole. In the first part, the location of the dipole has been assumed to vary in the horizontal and vertical directions beneath the heated surface as shown in Fig. 1(a). Simulations have been carried out for two common boundary conditions of isothermal and constant heat flux. The cooling performance of the system has been evaluated for

both cases separately. The effect of multiple magnetic field sources on the convective heat transfer has been investigated in the second part as shown in Fig. 1(b). Moreover, using genetic algorithm, the optimum arrangement of the dipoles have been obtained in order to achieve the maximum heat transfer rate.

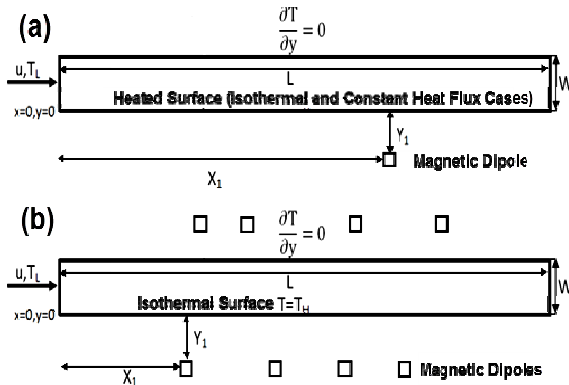


Fig. 1. Schematic of the studied problems

Governing Equations

Magnetic Body Force

Gauss's law for the magnetic flux density is:

$$\vec{B} = \mu_0(\vec{M} + \vec{H}) \quad (1)$$

where, H and M are magnetic field and magnetization, respectively.

Ampere's law with zero current density assumption is also stated as:

$$\vec{\nabla} \cdot \vec{B} = 0 \quad (2)$$

$$\vec{\nabla} \times \vec{H} = 0 \quad (3)$$

The magnetic field can be obtained from [4]:

$$\vec{H} = -\nabla V_m \quad (4)$$

where, V_m is the scalar magnetic potential. For a line dipole, it can be expressed as follows[11].

$$V_m(x, y) = \frac{m}{2\pi} \frac{x-X}{(x-X)^2 + (y-Y)^2} \quad (5)$$

Where m represents the strength of the magnetic field and X and Y are the locations of a single line dipole. Then, H is obtained in polar coordinates as

$$\vec{H}(r, \phi) = \frac{Y}{2\pi r^2} (\cos(2\phi) \vec{i} + \sin(2\phi) \vec{j}) \quad (6)$$

Where r and ϕ are defined as:

$$r = \sqrt{(x-X)^2 + (y-Y)^2} \quad (7)$$

$$\phi = \tan^{-1} \left(\frac{y-Y}{x-X} \right) \quad (8)$$

The magnetic field and magnetization vector are related as follows.

$$\vec{M} = \chi_m \vec{H} \quad (9)$$

The variation of the total magnetic susceptibility, χ_m as a function of temperature is rewritten as[11]:

$$\chi_m = \chi_m(T) = \frac{\chi_0}{1 + \beta(T - T_0)} \quad (10)$$

where, χ_0 is the susceptibility at a reference temperature.

The corresponding Kelvin body force per volume for a ferrofluid is defined as [4, 11]:

$$\vec{F}_K = \vec{M} \cdot \nabla \vec{B} \quad (11)$$

Fluid Flow and Heat Transfer Equations

The governing equations for conservation of mass, momentum in x, y directions (Navier-Stokes equations) and energy are given by equations 12-15, respectively.

$$\frac{\partial u}{\partial x} + \frac{\partial v}{\partial y} = 0 \quad (12)$$

$$\frac{\partial u}{\partial t} + u \frac{\partial u}{\partial x} + v \frac{\partial u}{\partial y} = -\frac{1}{\rho} \cdot \frac{\partial P}{\partial x} + \frac{\mu}{\rho} \left(\frac{\partial^2 u}{\partial x^2} + \frac{\partial^2 u}{\partial y^2} \right) + F_K(x) \quad (13)$$

$$\frac{\partial v}{\partial t} + u \frac{\partial v}{\partial x} + v \frac{\partial v}{\partial y} = -\frac{1}{\rho} \cdot \frac{\partial P}{\partial y} + \frac{\mu}{\rho} \left(\frac{\partial^2 v}{\partial x^2} + \frac{\partial^2 v}{\partial y^2} \right) + F_K(y) \quad (14)$$

$$\frac{\partial T}{\partial t} + u \frac{\partial T}{\partial x} + v \frac{\partial T}{\partial y} = \alpha \left(\frac{\partial^2 T}{\partial x^2} + \frac{\partial^2 T}{\partial y^2} \right) + \mu \theta \quad (15)$$

where, θ is the viscous dissipation and is calculated from:

$$\theta = 2 \left(\frac{\partial u}{\partial x} \right)^2 + 2 \left(\frac{\partial v}{\partial y} \right)^2 + \left(\frac{\partial v}{\partial x} + \frac{\partial u}{\partial y} \right)^2 \quad (16)$$

The foregoing equations are non-dimensionalized using the following parameters:

$$x^* = \frac{x}{W}, \quad y^* = \frac{y}{W} \quad (17)$$

$$u^* = \frac{u}{u_{ref}}, \quad v^* = \frac{v}{u_{ref}} \quad (18)$$

$$t^* = \frac{t u_{ref}}{W} \quad (19)$$

$$P^* = \frac{P}{\rho u_{ref}^2} \quad (20)$$

$$T^* = \frac{T - T_0}{T_H - T_0} \quad (21)$$

Using Eq.17-21, Eq.12-15 can be rewritten as:

$$\frac{\partial u^*}{\partial x^*} + \frac{\partial v^*}{\partial y^*} = 0 \quad (22)$$

$$\frac{\partial u^*}{\partial t^*} + u^* \frac{\partial u^*}{\partial x^*} + v^* \frac{\partial u^*}{\partial y^*} = -\frac{\partial P^*}{\partial x^*} + \frac{1}{Re} \left(\frac{\partial^2 u^*}{\partial x^{*2}} + \frac{\partial^2 u^*}{\partial y^{*2}} \right) + F_K^*(x^*) \quad (23)$$

$$\frac{\partial v^*}{\partial t^*} + u^* \frac{\partial v^*}{\partial x^*} + v^* \frac{\partial v^*}{\partial y^*} = -\frac{\partial P^*}{\partial y^*} + \frac{1}{Re} \left(\frac{\partial^2 v^*}{\partial x^{*2}} + \frac{\partial^2 v^*}{\partial y^{*2}} \right) + F_K^*(y^*), \quad (24)$$

$$\frac{\partial T^*}{\partial t^*} + u^* \frac{\partial T^*}{\partial x^*} + v^* \frac{\partial T^*}{\partial y^*} = \frac{1}{Re Pr} \left(\frac{\partial^2 T^*}{\partial x^{*2}} + \frac{\partial^2 T^*}{\partial y^{*2}} \right) + \frac{Ec}{Re} \theta^*. \quad (25)$$

It should be noted that effective values for the properties of ferrofluid are used in the above equations.

Finally, Nusselt number is defined as:

$$Nu = \frac{-2\partial T^*/\partial y^*}{1-T_m^*} \quad (26)$$

Where T_m^* is the mean temperature that can be calculated for a fluid with constant properties using Eq. 27.

$$T_m^* = \frac{\int_A u^* T^*}{\int_A u^*}, \quad (27)$$

where, A is the cross-section of the channel perpendicular to the channel plane.

Numerical Solution

Ferrofluid enters the channel with a uniform velocity and temperature and the flow is considered laminar and fully developed at the exit. The thermal properties of the fluid are assumed to be constant, and the buoyancy effects are negligible compared with the forced convection and hydromagnetic effects. It is also assumed that the fluid is non-conducting.

The set of two-dimensional governing equations are solved using finite volume method. The solver specifications for the discretization of the domain involve the presto, second-order upwind, first-order upwind and second-order for pressure, momentum, and energy, respectively. Furthermore, no-slip condition is applied for both bottom and top surfaces.

A structured non-uniform grid is used to discretize the computational domain. The grid points are clustered near the channel walls and in the entrance region where the velocity and temperature gradients are large. The effects of different grid sizes on the Nusselt number along the channel are studied. Fig. 2 shows the variation of the Nusselt number on the bottom surface obtained from different grid sizes.

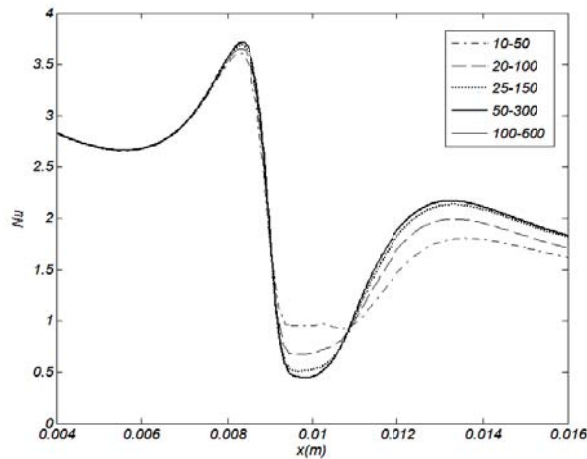


Fig. 2. Grid independency test

As shown, the last two grid systems lead to almost the same results. Thus, the grid of 300×50 (x, y) is used in the simulations.

Results and Discussion

A water-based ferrofluid with inlet temperature and Reynolds number of 300 K and 10, respectively is considered in the simulations. The ferrofluid properties are summarized in Table 1.

Table 1. Ferrofluid properties

Property	Value	Property	Value
ρ	1180 kg/m ³	χ_0	0.06
C_p	4000 J/kg	γ	0.01 A.m
μ	10 ⁻³ Ns/m ²	β	5.6 × 10 ⁻⁴ 1/K
Pr	5.5	k	0.7273

In order to demonstrate the validity and precision of the numerical procedure, a comparison has been made with the previously published work in the field of ferrohydrodynamics. Fig. 3 indicates the variation of Nusselt number in a channel surface for two different values of magnetic field strength, $m_1 = 0.19$ and $m_2 = 0.58$ Am.

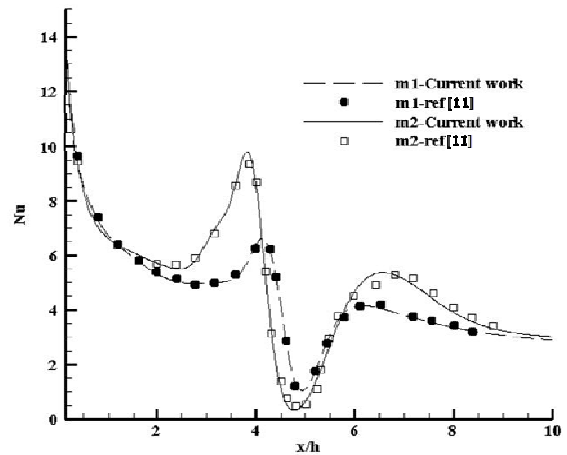


Fig. 3. Validation of the numerical results

As shown, the code has predicted the magnetic field effect appropriately.

In order to illustrate the features of ferrofluid flow under the influence of a magnetic dipole, a primary simulation is carried out with two dipoles placed at $X^* = 4$ beneath the bottom surface and $X^* = 6$ above the top surface. The streamlines and contours of non-dimensional x-velocity and temperature are plotted in Fig. 4.

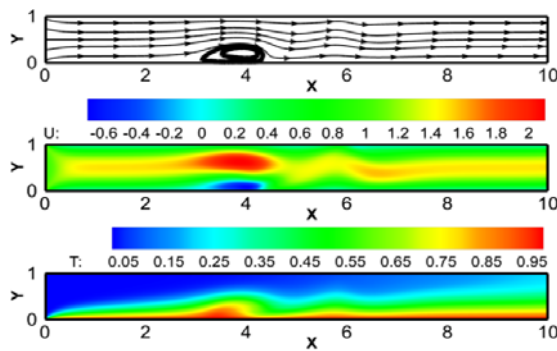


Fig. 4. Streamlines and contours of non-dimensional x-velocity and temperature for the sample case

As shown, the magnetic field of the bottom dipole has resulted in production of a local vortex near the heated surface. This is due to the temperature dependence of the magnetic susceptibility and resultant non-symmetrical magnetic body forces [3]. The vortices have great influence on the thermal boundary layer thickness. Thickening of the thermal boundary layer is observed in locations where direction of the flow in the vortex is along the direction of the mean flow. By contrast, thermal boundary layer shrinks in locations where the mean flow is in the opposite direction of the flow in vortex region. These two phenomena result in the decrease and increase of heat transfer rate, respectively. However, the second effect is dominant and heat transfer is expected to increase due to the magnetic field.

It should be also noted that, since a portion of the channel is blocked by the created vortex, the fluid reaches higher velocities above the vortex due to the continuity. This is clearly shown in x-velocity contours of Fig. 4.

Another interesting point is the difference between effects of two dipoles on the flow and temperature fields despite having the same magnetic field strength. In contrast with the bottom dipole, the dipole that is located above the top surface at $X^* = 6$ has less effect on streamlines and it has not led to formation of any vortex. This behavior can be attributed to the lower temperature gradient near the top dipole.

In order to quantify the foregoing discussion, Nusselt number for the sample case is calculated from Eq. 24 and is compared with the case with no magnetic field in Fig. 5.

A considerable decrease in the local Nusselt number on the left of the bottom dipole is observed which is the result of thickening of thermal boundary layer. However, the Nusselt number increases right after the center of the vortex. Although the second dipole has not resulted in formation of another vortex, it has affected the flow field and the heat transfer rate. The second drop and rise in the Nusselt number in Fig. 3 is due to the manipulation of the fluid flow by the second line dipole at $X^* = 6$. As discussed earlier, the second dipole has less impact on the ferrofluid since it is located above the adiabatic surface

where the temperature gradient is not as great as the isothermal bottom surface.

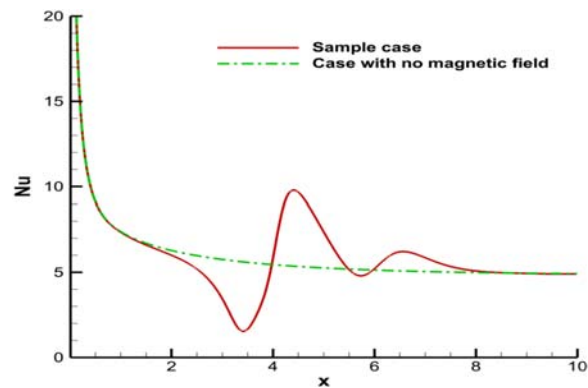


Fig. 5. Variation of Nusselt number on the bottom surface for the sample case compared with the case with no magnetic field

It is observed in Figs. 4 and 5 that a single magnetic field leads to thickening and shrinkage of the thermal boundary layer which have negative and positive effects on the heat transfer enhancement, respectively. Therefore, location of the magnetic field source and thermal boundary layer thickness at that point determine which effect dominates. Moreover, interaction of multiple magnetic fields can lead to different temperature fields and heat transfer rates.

Single Magnetic Field Source

In order to investigate the effect of position of the magnetic field source on the heat transfer from the heated surface, location of the magnetic line dipole is varied in the grid of $0.004m \leq x \leq 0.016m$ and $-0.0020m \leq y \leq -0.0010m$ below the heated surface with a $0.0001m$ increment. The magnetic moment of the dipole is $0.07Am$. Numerical simulations have been carried out for isothermal and constant heat flux boundary conditions, separately.

Isothermal Boundary Condition

The temperature of the heated surface is kept constant at $380K$. Variation of the local Nusselt number for different horizontal and vertical locations of the line dipole has been calculated and compared with the case of no magnetic field in Figs. 6(a) and (b).

It is observed in Fig.6(a) that the maximum value of the Nu decreases with the distance of line dipole from the channel entrance. This can be justified considering the fact that the thermal boundary layer grows with x. In other words, the effect of magnetic field in shrinking the boundary layer and drawing the cold fluid to the hot wall is less pronounced for larger boundary layer thicknesses. Moreover, Nu decays as the vertical distance from the heated plate increases, as shown in Fig.6(b).

In order to find the optimum magnetic dipole location, the total heat transfer rate has been calculated by integrating the heat flux over the specified length for all simulated cases. Variation of the total heat transfer from the heated bottom surface with respect to x and y coordinates is shown in Fig. 7.

The total heat transfer rate for the case of no magnetic field is calculated as 739.14 W. Thus, it can be concluded from Fig.7 that magnetic field does not necessarily lead to convection heat transfer enhancement since for some points, the calculated value is less than 739.14 W. From the distribution of the total heat transfer rate, the optimum location of the line dipole is found to be $(x, y) = (0.0053, -0.001)$. At this point, the heat transfer rate equals to 1099.72 W. Therefore, 49% enhancement in heat transfer rate can be achieved by placing the dipole at this point.

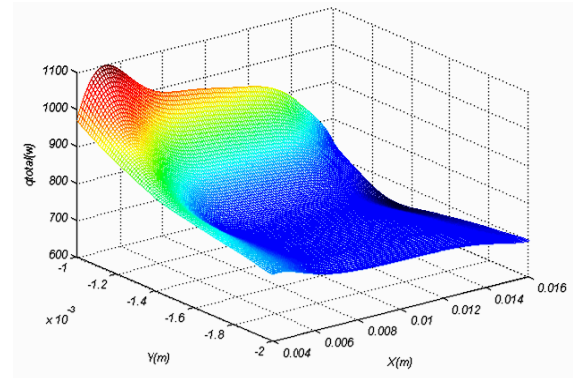


Fig. 7. Variation of the total heat transfer from the heated bottom surface with respect to x and y coordinates

Constant Heat Flux Boundary Condition

The above procedure has been repeated for finding the optimum dipole location when the lower wall is exposed to a constant heat flux of 50000 W/m^2 .

The effect of horizontal and vertical displacement of the line dipole on the temperature distribution on the bottom surface is shown in Figs. 8(a) and (b), respectively.

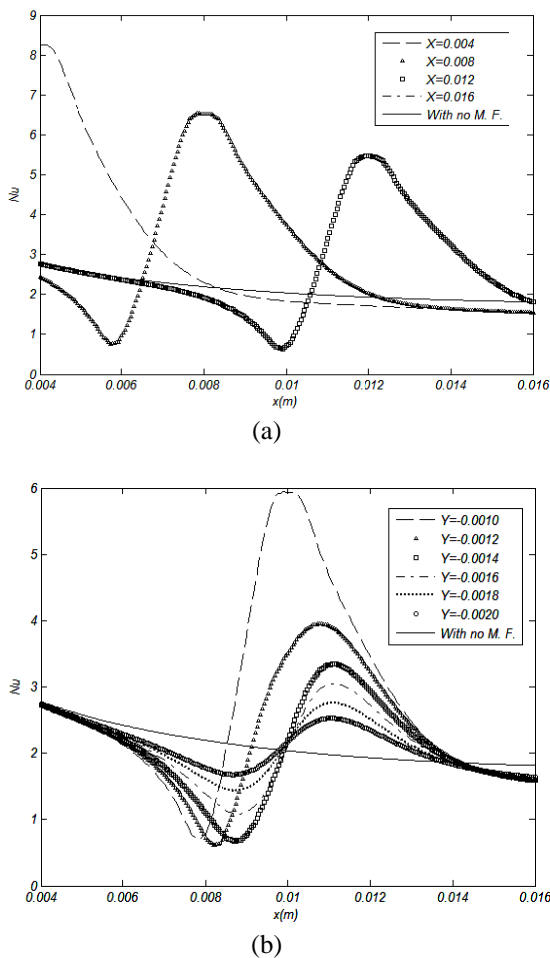


Fig. 6. (a) Variation of local Nusselt number for different horizontal positions of the dipole at $Y = -0.0010 \text{ m}$, (b) Variation of local Nusselt number for different vertical positions of the dipole at $X = 0.010$

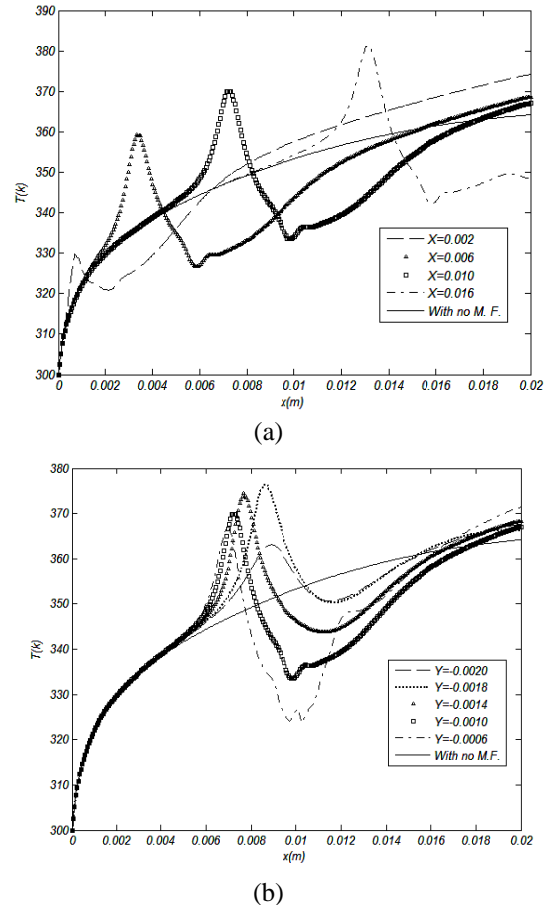


Fig. 8. (a) Temperature distribution on the constant heat flux surface for different horizontal positions of the dipole at $Y = -0.0010$, (b) Temperature distribution on the constant heat flux surface for different vertical positions of the dipole at $X = 0.010$

For the constant heat flux boundary condition, the main goal of the cooling system is to lower the temperature of the heated surface as much as possible. Therefore, the mean temperature of the heated surface can be a measure of system efficiency. Values of mean temperature on the heated surface have been calculated for all magnetic dipole locations and results are shown in Fig. 9.

Without a magnetic field, the mean temperature is calculated as 349.39K. It is shown in Fig. 9 that for some locations, magnetic field has increased the mean temperature. Therefore, placing a line dipole in such locations does not lead to a better cooling of the heated surface. On the other hand, for most of the locations near the heated surface, the heat transfer enhancement is achieved. The optimum source location is found to be $(x,y)=(0.0032,-0.0005)$.

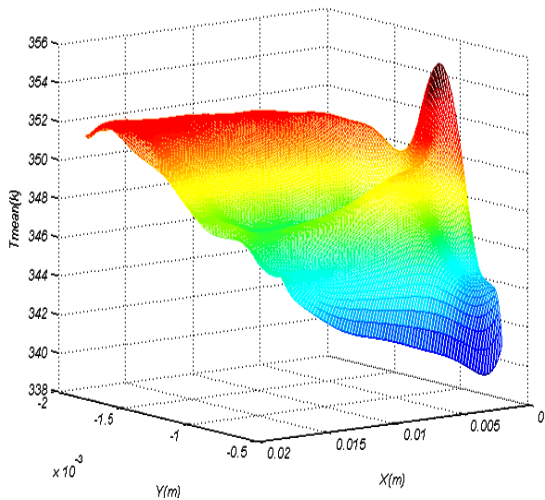


Fig. 9. Variation of the mean temperature on the heated bottom surface with respect to x and y coordinates

Ferro Fluid Heat Transfer Optimization Using Genetic Algorithm

In the second part, using genetic algorithm (GA) an optimum arrangement for multiple magnetic dipoles is found in order to achieve the maximum enhancement in heat transfer from the channel bottom surface. Four line dipoles are placed above the top and four line dipoles beneath the bottom surface.

As described previously, magnetic field has two opposite effects on the thermal boundary layer which are thickening and reformation of thermal boundary layer by disturbing it. The main idea behind optimization of the distribution of line dipoles is to find the total magnetic field that leads to the minimum drop in the Nusselt number, i.e. decreasing the negative effect due to the presence of line dipoles while maximizing the benefits of using the line dipoles.

The average Nusselt number for the bottom surface is chosen as the fitness function. The Convergence history of the optimization is plotted in Fig. 10.

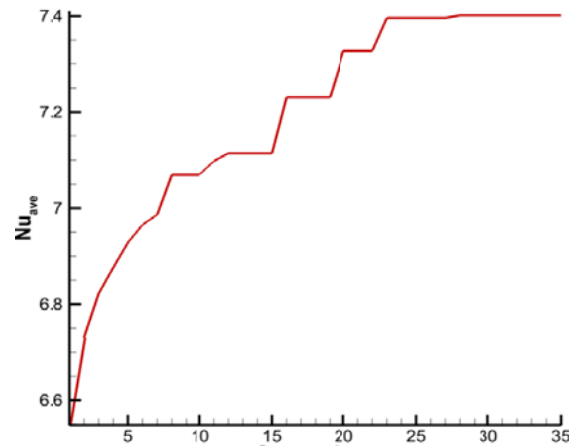


Fig. 10. Convergence history of the genetic algorithm for the average Nusselt number

As shown, the optimization process is converged after 27 generations. The optimum locations of the dipoles are found to be $X_1^* = 4, X_2^* = 4.8, X_3^* = 5.2$ and $X_4^* = 5.8$ beneath the bottom surface and $X_5^* = 4.4, X_6^* = 4.5, X_7^* = 4.7$ and $X_8^* = 4.8$ above the top surface.

Streamlines and contours of non-dimensional velocity and temperature for the optimal solution are plotted in Fig. 11.

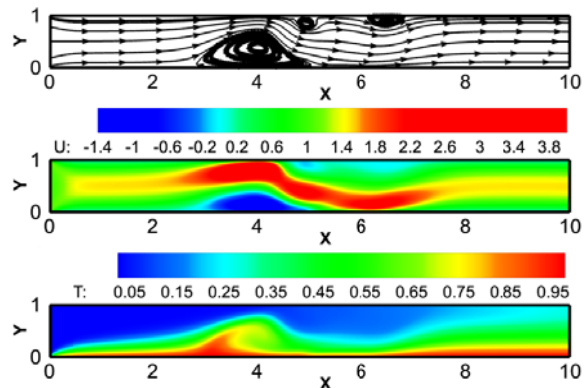


Fig. 11. Streamlines and contours of non-dimensional x-velocity and temperature for the optimal solution

The magnetic field created by the line dipoles results in the creation of three vortices as indicated in Fig. 11. The first vortex which is the largest, partially blocks the path of incoming fluid. Hence, the velocity of the incompressible fluid that passes above the vortex increases dramatically. Then, the fast streaming fluid is directed to pass along the hot bottom surface due to the body force that is imposed on ferrofluid by the magnetic field. The small vortex above the fluid that is directed to the bottom surface keeps the cross-section of the passing fluid small and velocity remains high, as a result. The manipulation of the flow field directly affects the thermal boundary layer above the bottom surface as illustrated in Fig. 11. It is clearly

shown that thermal boundary layer in right side of the main vortex is reformed and remained thin until the high velocity ferrofluid is detached from the bottom surface. Also, it should be noted that the dead zone in left of the main vortex center results in the growth of thermal boundary layer which would lead to poor heat transfer rate at that location.

In order to show the effect of the applied magnetic field on the heat transfer rate, the Nusselt number for the optimal case and the case with no magnetic field are plotted in Fig. 12.

As explained earlier, the sudden drop in the Nusselt number is due to the thick thermal boundary layer where the direction of velocity of the flow in the main vortex is in opposite direction of the main fluid flow. However, this is almost the only region where the Nusselt number of the optimal case is less than the Nusselt number of the original flow. In all other regions, the distribution of the magnetic field is such that the negative effect of using line dipoles (thickening of thermal boundary layer in the dead zones) is overcome and the thermal boundary layer is kept thin for a long distance. As a result, the average Nusselt number for the optimal magnetic field would reach 7.4 which shows a 27.6% increase compared to the original case with no magnetic field.

It is also possible to define the maximum bulk temperature at the exit as the objective. Fig. 13 illustrates change of the non-dimensional mean temperature for the optimal case compared with the case with no magnetic field.

In the absence of magnetic field, the bulk temperature behaves linearly after the thermal entry length as expected of the constant surface temperature boundary condition. However, applying the magnetic field by line dipoles disturbs the thermal boundary layer. Again, after a drop in the left side of the main vortex, the mean temperature is of the optimal design is greater than the original case, which means that the hot bottom surface has transferred more heat into the fluid that passes over it.

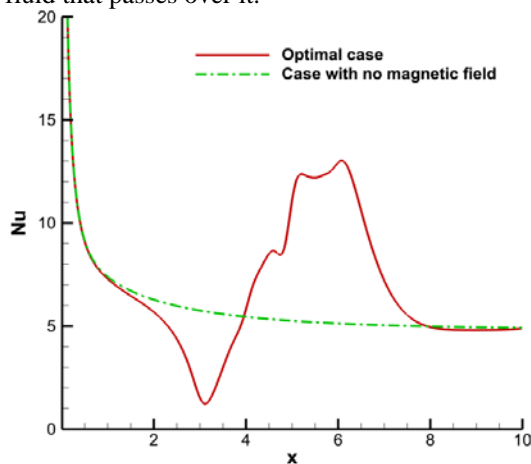


Fig. 12. The Nusselt number for the optimal case compared with the case with no magnetic field along the channel

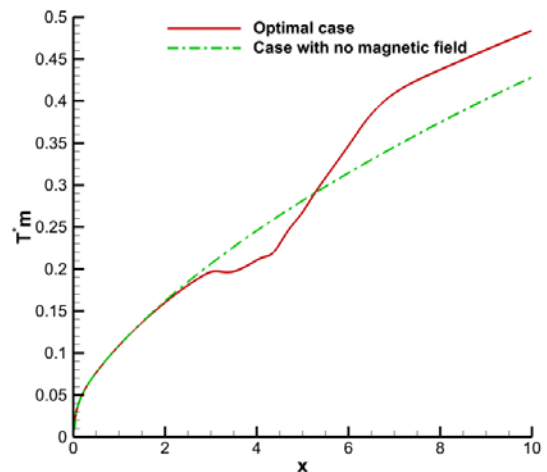


Fig. 13. Mean temperature for the optimal case compared with the case with no magnetic field along the channel

Conclusion

The effect of the magnetic field source location on the convective heat transfer of ferrofluid in a heated channel is investigated for isothermal and constant heat flux boundary conditions. Results show that placing a magnetic field in an arbitrary point near the channel does not necessarily lead to convective heat transfer enhancement. On the other hand, for some locations, the augmentation of the heat transfer is reflected in terms of increase in total heat transfer and decrease in mean temperature of the heated surface for isothermal and constant heat flux conditions, respectively. It was also shown that in contrast to the isothermal case, heat transfer does not always decrease with the magnetic field distance from the heated surface for constant heat flux condition. Next, using genetic algorithm, an optimum arrangement has been obtained for a set of eight magnetic field sources. It is shown that the flow and temperature fields can be manipulated by the application of multiple magnetic field sources. It is shown that a maximum 27 percent enhancement in Nusselt number can be achieved by proper arrangement of a set of eight dipoles below the studied channel and on the top of it.

References

- [1] Rinaldi, C., Chaves, A., Elborai, S., He, X. T. and Zahn, M., "Magnetic fluid rheology and flows," *Current Opinion in Colloid & Interface Science*, Vol. 10, 2005, pp. 141-157.
- [2] Finlayson, B., "Convective instability of ferromagnetic fluids," *Journal of Fluid Mechanics*, Vol. 40, 1970, pp. 753-767.
- [3] Odenbach, S., "Microgravity experiments on thermomagnetic convection in magnetic fluids," *Journal of magnetism and magnetic materials*, Vol. 149, 1995, pp. 155-157.

- [4] Rosensweig, R.E., *Ferrohydrodynamics*: Courier Corporation, 2013.
- [5] Selimefendigil, F., Öztop, H.F. and Al-Salem, K., "Natural convection of ferrofluids in partially heated square enclosures", *Journal of magnetism and magnetic materials*, Vol. 372, 2014, pp. 122-133.
- [6] Mojumder, S., Saha, S. and Mamun, M.A.H., "Effect of Magnetic Field on Natural Convection in a C-shaped Cavity Filled with Ferrofluid," *Procedia Engineering*, Vol. 106, 2015, pp. 96-104.
- [7] Krakov, M., Nikiforov, I. and Reks, A., "Influence of the uniform magnetic field on natural convection in cubic enclosure: experiment and numerical simulation," *Journal of magnetism and magnetic materials*, Vol. 289, 2005, pp. 272-274.
- [8] Sawada, T., Kikura, H., Saito, A. and Tanahashi, T., "Natural convection of a magnetic fluid in concentric horizontal annuli under nonuniform magnetic fields," *Experimental thermal and fluid science*, Vol. 7, 1993, pp. 212-220.
- [9] Aminfar, H., Mohammadpourfard, M. and Kahnamouei, Y. N. "A 3D numerical simulation of mixed convection of a magnetic nanofluid in the presence of non-uniform magnetic field in a vertical tube using two phase mixture model," *Journal of Magnetism and Magnetic Materials*, Vol. 323, 2011, pp. 1963.
- [10] Aminfar, H., Mohammadpourfard, M. and Zonouzi, S. A., "Numerical study of the ferrofluid flow and heat transfer through a rectangular duct in the presence of a non-uniform transverse magnetic field," *Journal of Magnetism and Magnetic materials*, Vol. 327, 2013, pp. 31-42.
- [11] Ganguly, R., Sen, S. and Puri, I. K., "Heat transfer augmentation using a magnetic fluid under the influence of a line dipole," *Journal of Magnetism and Magnetic Materials*, Vol. 271, 2004, pp. 63-73.
- [12] Streck, T. and Jopek, H., "Computer simulation of heat transfer through a ferrofluid," *Physica status solidi (b)*, Vol. 244, 2007, pp. 1027-1037.
- [13] Xuan, Y., Li, Q. and Ye, M., "Investigations of convective heat transfer in ferrofluid microflows using lattice-Boltzmann approach," *International Journal of Thermal Sciences*, Vol. 46, 2007, pp. 105-111.
- [14] Goharkhah, M. and Ashjaee, M., "Effect of an alternating nonuniform magnetic field on ferrofluid flow and heat transfer in a channel," *Journal of Magnetism and Magnetic Materials*, Vol. 362, 2014, pp. 80-89.
- [15] Ghasemian, M., Ashrafi, Z. N., Goharkhah, M. and Ashjaee, M., "Heat transfer characteristics of Fe₃O₄ ferrofluid flowing in a mini channel under constant and alternating magnetic fields," *Journal of Magnetism and Magnetic Materials*, Vol. 381, 2015, pp. 158-167.
- [16] Sheikhejad, Y., Hosseini, R. and Saffar-avval, M., "Effect of different magnetic field distributions on laminar ferroconvection heat transfer in horizontal tube", *Journal of Magnetism and Magnetic Materials*, Vol. 389, 2015, pp. 136-143.
- [17] Sheikhejad, Y., Hosseini, M., Teixeira, Shahpari, A., Hosseini, A. Saffar, R. and Avval, M., "Experimental Investigation and Three-Dimensional Numerical Analysis of Ferroconvection Through Horizontal Tube Under Magnetic Field of Fixed Parallel Magnet Bars," *Journal of Heat Transfer*, Vol. 139, 2017, pp. 131-141.
- [18] Tzirtzilakis, E., "A mathematical model for blood flow in magnetic field," *Physics of fluids*, Vol. 17, 2005, p. 077103.
- [19] Tzirtzilakis, E. and Kafoussias, N., "Three-dimensional magnetic fluid boundary layer flow over a linearly stretching sheet," *Journal of Heat Transfer*, Vol. 132, 2010, p. 011702.
- [20] Tzirtzilakis, E. and Tanoudis, G., "Numerical study of biomagnetic fluid flow over a stretching sheet with heat transfer," *International Journal of Numerical Methods for Heat & Fluid Flow*, Vol. 13, 2003, pp. 830-848.